Transportation Research Interdisciplinary Perspectives 21 (2023) 100858

Contents lists available at ScienceDirect

Transportation Research Interdisciplinary Perspectives

journal homepage: www.elsevier.com/locate/trip

Non-homogeneous traffic characterization based on driver reaction and stimuli

Waheed Imran [a,*], Zawar H. Khan [b], T. Aaron Gulliver [b], Muhammad Alam [c], Khurram S. Khattak [d]

[a] Department of Civil, Architectural and Environmental Engineering, University of Naples, Federico II, Via Claudio 21, 80125, Italy
[b] Department of Electrical and Computer Engineering, University of Victoria, PO Box 1700, STN CSC, Victoria, BC, Canada V8W 2Y2
[c] Department of Civil Engineering, University of Engineering and Technology, Mardan 25000, Pakistan
[d] Department of Computer Systems Engineering, University of Engineering and Technology, Peshawar 25000, Pakistan

ARTICLE INFO

Keywords:
Macroscopic model
Transition distance
Equilibrium velocity distribution
FORCE scheme
Non-homogeneous traffic

ABSTRACT

A macroscopic model for non-homogeneous traffic is proposed based on harmonization during transitions. This model considers the lateral and forward distances between vehicles, reaction and harmonization times, and changes in velocity. Further, the equilibrium velocity distribution is characterized based on the density and travel time of real non-homogeneous traffic. The proposed and Payne–Whitham (PW) models are evaluated over a 200 m circular road using the FORCE scheme. The results obtained demonstrate that the proposed model provides a more realistic representation of non-homogeneous traffic.

1. Introduction

Understanding traffic flow is important from both economic and societal perspectives. The economic factors include fuel consumption and travel time whereas the societal factors include driver fatigue and injuries (Imran et al., 2020). Congestion results in significant losses in both developing and developed countries (Timilsina and Dulal, 2010). Thus, techniques should be developed to overcome this problem. Traffic can be homogeneous or non-homogeneous. Homogeneous traffic follows lane discipline and is comprised of similar types of vehicles. In this case, there is little variation in velocity and density. Conversely, non-homogeneous traffic does not follow lane discipline and is often comprised of both motorized and non motorized vehicles (Mallikarjuna and Rao, 2011). This impedes traffic flow and often results in moving bottlenecks and congestion (Zhang, 1998). Non-homogeneous traffic is more complex than homogeneous traffic which makes flow characterization challenging (Delitala and Tosin, 2007). However, understanding this type of traffic is essential to designing effective strategies for traffic control (Jiang et al., 2002).

Spatial changes in traffic result in driver interactions (Khan et al., 2020). In particular, a safe distance is maintained with leading vehicles to prevent accidents (Brackstone and McDonald, 2007) and the distances between vehicles affect the traffic flow. Congested traffic is characterized by small distances between vehicles and high acceleration (Qu et al., 2014). Traffic flow is also affected by the lateral separation between vehicles. In a non-homogeneous flow, lateral distances can vary greatly as drivers do not maintain lane discipline. Therefore, a model considering both forward and lateral distances is required to adequately characterize non-homogeneous traffic.

Numerous traffic models have been developed to study traffic behavior. However, they cannot be used for non-homogeneous traffic since this type of traffic has not been explicitly incorporated. Further, vehicle behavior is often described by non-physical constants that do not reflect reality. Traffic models should be based on traffic physics. This is important as traffic in developing countries such as Pakistan is non-homogeneous. In this paper, a new macroscopic model that can be employed for non-homogeneous traffic is proposed. Both the forward and lateral distances between vehicles are used to characterize traffic behavior. The main contributions of this paper are as follows.

1. The well-known Payne–Whitham (PW) model is modified to incorporate the forward and lateral distances between vehicles. Thus, driver presumption is not a constant as in the PW model. Further, the parameters in the proposed model are based on traffic physics.
2. Regression models are used to characterize the velocity–density relationship (equilibrium velocity distribution), of non-homogeneous traffic based on real density and travel time data from a highway in Pakistan. These models are employed to characterize traffic behavior.

* Corresponding author.
E-mail addresses: waheedemran@hotmail.com (W. Imran), khanz@uvic.ca (Z.H. Khan), agullive@ece.uvic.ca (T.A. Gulliver), emalam82@gmail.com (M. Alam), khurram.s.khattak@gmail.com (K.S. Khattak).

https://doi.org/10.1016/j.trip.2023.100858
Received 15 August 2022; Received in revised form 16 February 2023; Accepted 5 June 2023
Available online 15 June 2023

3. A 200 m circular road with an inactive bottleneck is used to evaluate the performance of the proposed and PW models. In particular, the impact of lateral distance on the velocity is determined. The results obtained indicate that the proposed model provides a more realistic representation of non-homogeneous traffic.

The rest of this paper is organized as follows. A review of the related literature is presented in Section 2. The empirical equilibrium velocity distributions are given in Section 3. Section 4 presents the proposed macroscopic traffic model and the model hyperbolicity is examined in Section 5. The performance of the proposed and PW models is evaluated in Section 6. Finally, some conclusions are given in Section 7.

2. Literature review

Aggregate parameters such as velocity, density, and flow are typically examined using macroscopic traffic models (Kessels, 2019). Conversely, individual vehicle behavior is considered in microscopic models along with human behavior (Nagel et al., 2003) such as psychological and physical responses (Henein and White, 2010). Mesoscopic models combine the characteristics of both microscopic and macroscopic models (Cantarella et al., 2014) and probability distributions are often employed (Kessels, 2019; Hoogendoorn and Bovy, 2001). Macroscopic models are commonly used due to their low computational complexity (Khan et al., 2019b, 2022a).

The macroscopic study of traffic flow started with the Lighthill, Whitham and Richards (LWR) model (Lighthill and Whitham, 1955; Richards, 1956) which is given by

$$\rho_t + \rho(v(\rho))_x = 0, \tag{1}$$

where ρ is density and $v(\rho)$ is the relationship between velocity and density during equilibrium traffic conditions. The subscripts t and x represent spatial and temporal derivative, respectively. This model assumes traffic continuum and only small changes that occur instantaneously, i.e. ideal traffic conditions on a long road. This model cannot accurately characterize large or abrupt changes in traffic (Liu et al., 1998) such as in stop and go conditions or with rapid changes in velocity (Daganzo, 1995; Khan and Gulliver, 2018; Maerivoet and De Moor, 2008; Khan et al., 2022b). An acceleration term was added to improve the LWR model (Khan et al., 2019b). A higher-order traffic flow model based on car following theory was proposed by Payne (Zhang, 1998; Payne, 1971). It considers adjustments in traffic based on driver response (anticipation). An anticipation term was employed to characterize driver reaction to forward stimuli and a relaxation term to characterize changes in velocity (Maerivoet and De Moor, 2008). Whitham proposed a similar model and so it is known as the Payne Whitham (PW) model and is given by Khan and Gulliver (2019) and Khan et al. (2018)

$$\begin{aligned} \rho_t + \rho(v(\rho))_x &= 0, \\ (\rho v)_t + \left(\frac{(\rho v)^2}{\rho} + C_0^2\rho\right)_x &= \rho\left(\frac{v(\rho) - v}{\tau}\right), \end{aligned} \tag{2}$$

where C_0^2 is the velocity constant (backward perturbation propagation speed) and $\frac{v(\rho)-v}{\tau}$ is the relaxation term. This term characterizes traffic alignment during the relaxation time τ. The PW model assumes vehicles have uniform behavior (Whitham, 1971) which is contrary to reality as vehicle behavior varies according to factors such as traffic conditions. As a consequence, the PW model can produce unsatisfactory results (Zhang, 1998).

A model similar to the PW model was proposed in Kuhne and Rodiger (1991) and a numerical improvement of the PW model was given in Kerner and Konhäuser (1993). However, the diffusion terms and a constant backward perturbation propagation speed can cause unrealistic traffic behavior. A computationally efficient form of the PW model was proposed in Papageorgiou et al. (1989), but the parameters lack a physical interpretation so it is difficult to calibrate them. A macroscopic model based on the variance in the velocity was given in Helbing (1996). This model is based on Gas-Kinetic-Theory (GKT) so some parameters are difficult to interpret.

Del Castillo et al. (1994) incorporated anticipation and reaction time into the PW model. Phillips (1979) modeled the relaxation time τ as a function of traffic density. Daganzo (1995) demonstrated that traffic flow is affected by forward conditions and changes in velocity are smaller than the average velocity. The effect of leading vehicles is not considered in the PW model (Hegyi et al., 2001) and this can result in speeds below the minimum when the flow is large, which is unrealistic (Grace and Potts, 1964; Graham and Chenu, 1962). However, in multi lane traffic, lane speeds may differ which allows some vehicles to travel faster then the average speed (Papageorgiou, 1998).

Aw and Rascle (2000) improved the PW model by considering the density for changes at or below the average speed. However, the acceleration can be unrealistic when the density is high (Richardson, 2012). The time headway and lateral distance of vehicles in non-homogeneous traffic was considered in Imran et al. (2020), but the time headway is a constant. The PW model was improved in Khan et al. (2021) by incorporating gap filling behavior using analogies between traffic flow and the Maxwell–Boltzmann equation for gases. However, these analogies result in parameters not connected to the real world. These results indicate that existing models are not suitable for non-homogeneous traffic because changes during transitions are affected by the velocity and lateral distance between vehicles.

The relationship between average speed and traffic density under equilibrium conditions is given by the equilibrium velocity distribution (Jiang et al., 2002). When changes in flow occur, traffic moves towards this distribution. The velocity and density were considered in Bonzani and Mussone (2009) to develop equilibrium velocity distribution models. Greenshields proposed a distribution with an inverse linear relationship between velocity and density (Khan et al., 2019b) which is given by

$$v(\rho) = v_m\left(1 - \frac{\rho}{\rho_m}\right), \tag{3}$$

where v_m is the maximum velocity and ρ_m is the maximum density. This distribution is not suitable for non-homogeneous traffic because spatial changes in traffic are nonlinear. In reality, the flow is a convex function of density and the flow increases with decreasing density (Li and Zhang, 2011). Greenberg (1959) considered a logarithmic relationship between speed and density based on analogies with fluid dynamics. However, the free flow speed tends to infinity when the density is small. Underwood proposed an exponential relationship based on data from the Merritt Parkway in Connecticut (Salter, 1996). However, the velocity can become zero for large densities which is a major shortcoming of this model.

Traffic in developing countries consists of both motorized and non-motorized vehicles so it is non-homogeneous. Existing models were developed based on homogeneous traffic so they are unsuitable for non-homogeneous traffic. Most consider the density and neglect individual vehicle speeds and dimensions. Therefore, it is necessary to develop models for the equilibrium velocity distribution based on the density and travel time of non-homogeneous traffic. This will provide more accurate results and better inform traffic engineers.

3. Empirical equilibrium velocity distributions for non-homogeneous traffic

In this section, equilibrium velocity distributions for non-homogeneous traffic based on density and travel time are developed. Data was obtained from a 200 m section of National Highway N-45 (National Highways of Pakistan, 2018) in Mardan, KPK, Pakistan. This highway connects four districts of the Khyber Pakhtunkhwa and has a high traffic density. There are two lanes of width 3.6 m in each direction.

Fig. 1. The video recording components including solar panels, cameras, monitor, DVR, and UPS used for recording traffic data on a 200 m road section.

Table 1
Vehicle types and numbers.

Type	Number
Van	12
Car	63
Motorbike	45
Rickshaw	18
Tow truck	8
Small truck	6
Jeep	2
Tractor	2
Heavy truck	5
Bus	7
Trailer	2

The data was collected using a system consisting of two CCTV cameras, a digital video recorder (DVR), solar panels for power, an uninterruptable power supply (UPS), and two poles to mount the cameras as shown in Fig. 1. The data was recorded from 1200 h to 1500 h (PST) on Monday, August 13, 2018, which is the peak time for traffic. The weather was clear with 28% humidity. Eleven different types of vehicles were observed which indicates non-homogeneous traffic conditions. The number of vehicles of each type is given in Table 1.

The traffic data recorded on the road section is summarized in Table 2 and the detailed data is given in Imran et al. (2020). As the road section for this study is 200 m, The first camera was installed at the start of the road section and the second camera at the end of the road section. These points were marked with lime to accurately determine the time. The recorded video was visually analyzed. Traffic behind the leading vehicles in the road section was counted at random time intervals. The density was determined by dividing the number of vehicles by 200 m. The ingress and egress times of the leading vehicles were also recorded. The travel time is the difference between these times and the velocity is 200 m divided by this time. The density, travel time, and velocity of some of the observed vehicles is given in Table 2. The maximum travel time of 42 s was for a trailer with a velocity of 4.8 m/s and density 35/200 veh/m.

The velocity of the vehicles on the road section in m/s is 200 m divided by the travel time and is given in Table 2. This gives the equilibrium velocity distribution

$$v(t) = 200/t, \tag{4}$$

for non-homogeneous traffic. The velocity versus density on the road section is given in Fig. 2. This shows that the velocity decreases as the density increases, as expected. The velocity is 20 m/s when the density is 1 veh/200 m and this decreases to 9 m/s when the density is 25 veh/200 m. This experimental data is used to determine the equilibrium velocity distribution for non-homogeneous traffic.

Table 2
Traffic data obtained on a 200 m road section.

Type	Ingress time (s)	Egress time (s)	Density (veh/200 m)	Travel time (s)	Velocity (m/s)	Velocity (km/h)
Van	1	11	1	10	20.0	72.0
Car	27	37	4	10	20.0	72.0
Motorbike	27	39	4	12	16.7	60.0
Rickshaw	54	74	6	20	10.0	36.0
Tow truck	59	70	6	11	18.2	65.5
Small truck	9	22	6	13	15.4	55.4
Car	52	62	7	10	20.0	72.0
Heavy truck	42	54	8	12	16.7	60.0
Jeep	59	75	9	16	12.5	45.0
Tractor	43	67	30	24	8.3	30.0
Bus	9	46	35	37	5.4	19.5
Trailer	49	91	35	42	4.8	17.1

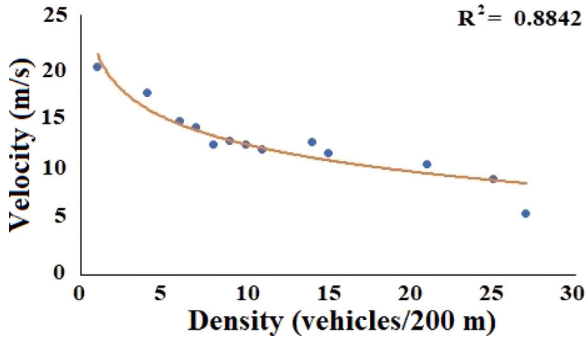

Fig. 2. Velocity versus density for the experimental traffic data from a 200 m road section with non-homogeneous traffic conditions.

To determine the best distribution for the velocity based on the density, the coefficient of determination (R^2), Mean Square Error (MSE), and Mean Absolute Error (MAE) are considered. The coefficient of determination is based on velocity v and density ρ and is given by

$$R = \frac{n(\sum_{i=1}^{n} v_i\rho_i) - (\sum_{i=1}^{n} v_i)(\sum_{i=1}^{n} \rho_i)}{\sqrt{\left(\left(n(\sum_{i=1}^{n} v_i^2 - (\sum_{i=1}^{n} v_i)^2)\right)\left(n(\sum_{i=1}^{n} \rho_i^2 - (\sum_{i=1}^{n} \rho_i)^2)\right)\right)}}, \tag{5}$$

where $n = 170$ is the number of observations. The MSE is

$$\text{MSE} = \left(\frac{\sum_{i=1}^{n}(p_i - o_i)^2}{n}\right), \tag{6}$$

where p_i is the ith predicted value and o_i is the corresponding observed value, and the MAE is

$$\text{MAE} = \frac{1}{n}\sum_{1}^{n}(|p_i - o_i|). \tag{7}$$

A robust model should have small MSE and MAE, and large R^2 (Devore, 2011). The coefficient of determination is a general measure while the MSE and MAE are typically used to compare different functions. The values of R^2, MSE, and MAE for logarithmic, exponential and linear functions are given in Table 3. These results indicate that the logarithmic function given by

$$v(\rho) = -3.76\ln(\rho) + 21.25, \tag{8}$$

is the best fit and this is shown in Fig. 2.

4. Extended PW model for non-homogeneous traffic

Transitions are changes in velocity due to changes in density (Yu et al., 2016) and occur during the transition time τ_t. Driver reaction to a transition can be expressed as

$$D_r = \frac{\Delta v}{\tau_t}, \tag{9}$$

Table 3
The coefficient of determination, mean squared error and mean absolute error for several density functions.

Function	Equation	R^2	MSE	MAE
Logarithmic	$-3.76\ln\rho + 21.25$	0.884	1.310	0.816
Exponential	$18.84e^{-0.035\rho}$	0.854	1.410	1.017
Linear	-0.402ρ+17.74	0.839	1.820	1.194

where Δv is the change in velocity to adjust to forward conditions. Reaction is quick with a small transition time, and vice versa for a large transition time (Xin and Xu, 2015). Assuming a constant velocity during a transition (Khan and Gulliver, 2020), the safe distance d_s is proportional to τ_t. Since a vehicle moves this distance during a transition (Qu et al., 2014), (9) can be reformulated as

$$D_r = \frac{\Delta v}{d_s}. \tag{10}$$

Further, drivers react according to the equilibrium velocity distribution $v(\rho)$. A larger difference in velocity between forward and following vehicles results in a greater reaction to align to forward vehicles. This difference is

$$\Delta v = |v(\rho) - v|, \tag{11}$$

and substituting this in (10) gives

$$D_r = \frac{|v(\rho) - v|}{d_s}. \tag{12}$$

Drivers maintain a safe transition distance between vehicles during equilibrium flow to avoid collisions with leading vehicles. When the transition distance is less than this, collisions are more likely to occur. The time to cover the safe transition distance is the reaction time τ_r to a forward change in traffic and the harmonization time τ_b to adjust to this change (Qu et al., 2014)

$$\tau_r + \tau_b. \tag{13}$$

Thus, τ_b is the stopping time and the stopping distance is

$$s = \frac{v^2}{2a_m}, \tag{14}$$

where a_m is the maximum deceleration. Thus, the safe transition distance is

$$d_s = v \times (\tau_r + \tau_b) + \frac{v^2}{2a_m}, \tag{15}$$

and substituting this in (12) gives

$$D_r = \frac{|v(\rho) - v|}{v \times (\tau_r + \tau_b) + \frac{v^2}{2a_m}}. \tag{16}$$

This indicates that a driver reacts to forward traffic changes by adjusting their velocity over the safe transition distance (Qu et al., 2014).

In non-homogeneous traffic, during congestion vehicles do not obey lane discipline (Mi et al., 2019) and the lateral distance between vehicles is small. When the traffic is free flow, lane discipline is typically followed and the lateral distance between vehicles is large. Thus, the speed increases as the density decreases and driver reaction is more likely to result in a smooth flow. In this paper, traffic stimulus is characterized by the ratio of average lateral distance to maximum lateral distance between vehicles (Imran et al., 2020)

$$\varsigma = \frac{b_a}{b_m}, \tag{17}$$

where b_a is the average lateral distance and b_m is the maximum lateral distance. ς is negligible when b_a is small and 1 when the maximum lateral distance between vehicles is achieved. Driver reaction to forward conditions is based on the traffic stimulus. For a large stimulus, there are large changes in vehicle speed at transitions whereas for a small stimulus this change is small. Thus, when ς is near 0, there is no driver reaction as the traffic flow is negligible, and when $\varsigma = 1$, driver reaction is large as the flow is high.

Driver response is the product of stimulus and driver reaction (Zhang, 1998). Using driver reaction from (16) and stimulus from (17) gives

$$v_r = \left(\frac{|v(\rho) - v|}{v \times (\tau_r + \tau_b) + \frac{v^2}{2a_m}} \right) \times \varsigma, \tag{18}$$

which indicates that velocity (speed) harmonization is based on the stimulus of forward traffic while maintaining a safe transition distance. For simplicity, let $f = \left(\frac{|v(\rho)-v|}{v\times(\tau_r+\tau_b)+\frac{v^2}{2a_m}} \right)$, and substituting (18) for C_0^2 in (2) gives the second equation for the proposed model

$$(\rho v)_t + \left(\frac{(\rho v)^2}{\rho} + f\varsigma\rho \right)_x = \rho \left(\frac{v(\rho) - v}{\tau} \right). \tag{19}$$

The first equation of the proposed model is the same as in the PW model (2). Eq. (19) indicates that traffic evolution in non-homogeneous traffic is based on driver response, driver reaction, and harmonization time. Conversely, traffic evolution with the PW model is the same regardless of the stimuli.

5. Traffic flow model hyperbolicity

Changes in flow during congestion are greater in downstream traffic than in upstream traffic. This condition is guaranteed by hyperbolicity, so traffic systems should be hyperbolic (Morgan, 2002; Khan et al., 2020). A system with real and distinct eigenvalues is strictly hyperbolic. The conserved form (small changes in traffic), of the models in vector form is

$$\chi_t + f(\chi)_x = S(\chi), \tag{20}$$

where the subscripts x and t denote spatial and temporal derivative, respectively, and

$$\chi = \begin{pmatrix} \rho \\ \rho v \end{pmatrix}, f(\chi) = \begin{pmatrix} \rho v \\ \frac{(\rho v)^2}{\rho} + {C_0}^2\rho \end{pmatrix}, S(\chi) = \begin{pmatrix} 0 \\ \rho\frac{v(\rho)-v}{\tau} \end{pmatrix}, \tag{21}$$

for the PW model (Khan et al., 2019b) and

$$\chi = \begin{pmatrix} \rho \\ \rho v \end{pmatrix}, f(\chi) = \begin{pmatrix} \rho v \\ \frac{(\rho v)^2}{\rho} + f\varsigma\rho \end{pmatrix}, S(\chi) = \begin{pmatrix} 0 \\ \rho\frac{v(\rho)-v}{\tau} \end{pmatrix}, \tag{22}$$

for the proposed model. For quasilinear systems, harmonization occurs only due to anticipation, so the relaxation term $S(\chi)$ is zero. Then (20) becomes

$$\chi_t + f(\chi) = 0. \tag{23}$$

The Jacobian matrix for the PW model is

$$A(\chi) = \begin{pmatrix} 0 & 1 \\ -v^2 + C_0^2 & 2v \end{pmatrix}, \tag{24}$$

and the eigenvalues are the solutions of

$$|A(\chi) - \lambda I| = \begin{vmatrix} -\lambda & 1 \\ -v^2 + C_0^2 & 2v - \lambda \end{vmatrix}, \tag{25}$$

which are (Khan et al., 2019a)

$$\lambda_1 = v + C_0, \qquad \lambda_2 = v - C_0. \tag{26}$$

These eigenvalues are real and distinct so the model is hyperbolic. The changes in traffic during congestion occur at below average velocity considering λ_2 whereas changes during free flow occur at higher speeds considering λ_1. This is because changes in velocity occur based on a constant C_0 regardless of the stimuli, which is not realistic.

The Jacobian matrix for the proposed model is

$$A(\chi) = \begin{pmatrix} 0 & 1 \\ -v^2 + f\varsigma & 2v \end{pmatrix}, \tag{27}$$

and the eigenvalues are the solutions of

$$|A(\chi) - \lambda I| = \begin{vmatrix} -\lambda & 1 \\ -v^2 + f\varsigma & 2v - \lambda \end{vmatrix}, \tag{28}$$

which are

$$\lambda_1 = v + \sqrt{f\varsigma}, \lambda_2 = v - \sqrt{f\varsigma}, \tag{29}$$

where

$$\sqrt{f\varsigma} = \sqrt{\left(\frac{|v(\rho) - v|}{v \times (\tau_r + \tau_b) + \frac{v^2}{2a_m}}\right)\frac{b_a}{b_m}}. \tag{30}$$

Substituting (30) in (29) gives

$$\lambda_1 = v + \sqrt{\left(\frac{|v(\rho) - v|}{v \times (\tau_r + \tau_b) + \frac{v^2}{2a_m}}\right)\frac{b_a}{b_m}}, \lambda_2 = v - \sqrt{\left(\frac{|v(\rho) - v|}{v \times (\tau_r + \tau_b) + \frac{v^2}{2a_m}}\right)\frac{b_a}{b_m}}. \tag{31}$$

To ensure hyperbolicity, the discriminant should be positive and distinct (Khan and Gulliver, 2018; Toro, 2011) and since this is satisfied by (31), the proposed traffic model (19) is hyperbolic. Further, these eigenvalues indicate that changes during harmonization are based on lateral distance headway, reaction, and harmonization time.

6. Performance results

The PW and proposed models are numerically discretized using the first order centered (FORCE) scheme (Khan et al., 2020). A 200 m circular road is considered to evaluate the performance. The simulation parameters are given in Table 4. The Courant, Friedrich and Lewy (CFL) (de Moura and Kubrusly, 2013) conditions are employed to ensure model stability. For the proposed model, the road and time steps are $\Delta x = 2$ m and $\Delta t = 0.01$ s, respectively. The simulation time for both models is 10 s and the target is the equilibrium velocity distribution. The maximum velocity is $v_m = 23$ m/s and the maximum normalized density is $\rho_m = 1$. τ_r ranges between 0.8 s to 1.0 s, and τ_b ranges between 0.1 s and 0.2 s (Basak et al., 2013; Yi et al., 2004). Thus, in this paper $\tau_r = 0.9$ s and $\tau_b = 0.2$ s are considered. The maximum deceleration is 7 ms^{-2} (Qu et al., 2014). The initial density at time $t = 0$ for the proposed and PW models is

$$\rho_0 = \begin{cases} 0.01, & \text{for } x \le 100 \\ 0.2, & \text{for } x \ge 100, \end{cases} \tag{32}$$

over the 200 m road. The speed constant (backward perturbation propagation speed) for the PW model varies between 2.4 m/s and 57 m/s (Khan et al., 2019b), so in this paper $C_0 = 5, 15$ and 20 m/s are utilized.

6.1. Proposed model velocity behavior using (8)

The proposed model velocity over the 200 m circular road at 1 s with $\varsigma = 0.1$ and $\varsigma = 0.5$, and target equilibrium velocity distribution given by (8) is shown in Fig. 3 and given in Table 5. With $\varsigma = 0.1$, at 1 m the velocity is 13.4 m/s and increases to 22.9 m/s at 48 m. It is 10.7 m/s at 120 m and increases to 13.1 m/s at 200 m. With $\varsigma = 0.5$, the velocity is 12.0 m/s at 1 m and increases to 22.3 m/s at 72 m. It is approximately 11.1 m/s from 150 m to 178 m and then increases to 11.8 m/s at 200 m. The corresponding velocity at 5 s is shown in Fig. 4 and given in Table 5. With $\varsigma = 0.1$, the velocity at 1 m is 11.9 m/s and is 16.7 m/s at 98 m and 11.9 m/s at 200 m. With $\varsigma = 0.5$, at 1 m the velocity is 11.5 m/s, increases to 18.1 m/s at 114 m, and then decreases to 11.5 m/s at 200 m. The corresponding velocity at 10 s is shown in Fig. 5 and given in Table 5. With $\varsigma = 0.1$, at 1 m the velocity is 13.1 m/s, increases to 14.8 m/s at 142 m, and then decreases to 13.4 m/s at 200 m. With $\varsigma = 0.5$, at 1 m the velocity is 13.6 m/s, increases to 15.7 m/s at 162 m, and then decreases to 13.7 m/s at 200 m.

Table 4
Simulation parameters.

Description	Value
Simulation time	10 s
Circular road length	200 m
v_m	23 m/s
Δt	0.01 s
Δx	2 m
Relaxation time	$\tau = 2.5$ s
Reaction time	$\tau_r = 0.9$ s
Harmonization time	$\tau_b = 0.2$ s
Velocity distribution	Greenshields, (4) and (8)
ρ_m	1
C_0	5 m/s, 15 m/s, and 20 m/s
Maximum deceleration, a_m	7 ms^{-2}

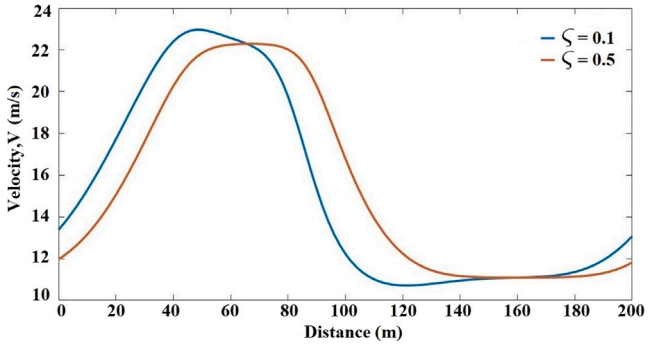

Fig. 3. The proposed model velocity over a 200 m circular road at 1 s with $\varsigma = 0.1$ and $\varsigma = 0.5$, and target equilibrium velocity distribution given by (8).

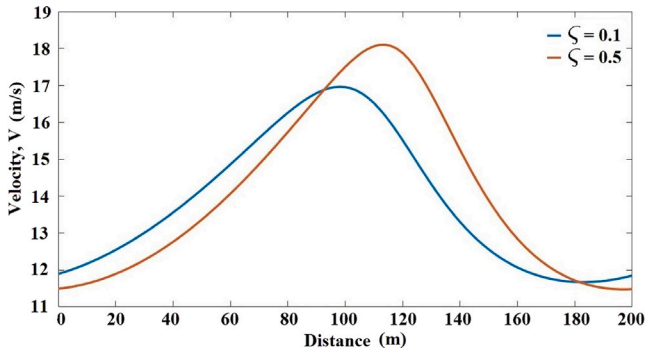

Fig. 4. The proposed model velocity over a 200 m circular road at 5 s with $\varsigma = 0.1$ and $\varsigma = 0.5$, and target equilibrium velocity distribution given by (8).

6.2. Proposed model velocity behavior using (4)

The proposed model velocity at 1 s over the 200 m circular road with $\varsigma = 0.1$ and $\varsigma = 0.5$, and target equilibrium velocity distribution given by (4) is shown in Fig. 6 and given in Table 6. With $\varsigma = 0.1$, at 1 m the velocity is 12.0 m/s and increases to 20.1 m/s at 142 m. It decreases to 10.1 m/s at 126 m and is 11.7 m/s at 200 m. With $\varsigma = 0.5$, at 1 m the velocity is 11.0 m/s and increases to 19.8 m/s at 70 m. It is approximately 10.3 m/s from 146 m to 178 m and is 10.9 m/s at 200 m. The corresponding velocity at 5 s is shown in Fig. 7 and given in

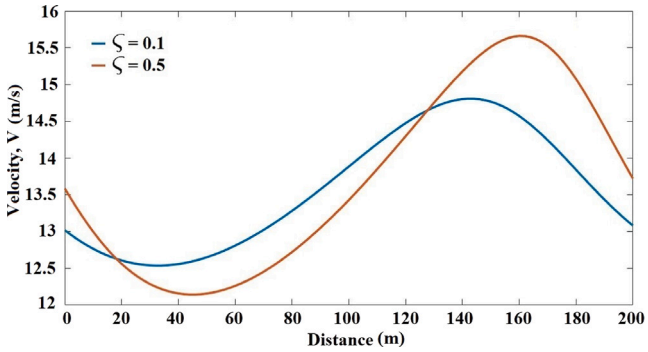

Fig. 5. The proposed model velocity over a 200 m circular road at 10 s with $\varsigma = 0.1$ and $\varsigma = 0.5$, and target equilibrium velocity distribution given by (8).

Table 5
The proposed model velocity with $\varsigma = 0.1$ and $\varsigma = 0.5$ at 1 s, 5 s, and 10 s, and target equilibrium velocity distribution given by (8).

Time (s)	ς	Distance (m)	Velocity (m/s)
1	0.1	1	13.4
1	0.1	48	22.9
1	0.1	120	10.7
1	0.1	200	13.1
1	0.5	1	12.0
1	0.5	72	22.3
1	0.5	120–178	11.1
1	0.5	200	11.8
5	0.1	1	11.9
5	0.1	98	16.7
5	0.1	200	11.9
5	0.5	1	11.5
5	0.5	114	18.1
5	0.5	200	11.5
10	0.1	1	13.1
10	0.1	142	14.8
10	0.1	200	13.1
10	0.5	1	13.6
10	0.5	162	15.7
10	0.5	200	13.7

Table 6. With $\varsigma = 0.1$, at 1 m the velocity is 10.8 m/s, increases to 15.5 m/s at 98 m, and then decreases to 11.0 m/s at 200 m. With $\varsigma = 0.5$, at 1 m the velocity is 10.6 m/s, increases to 16.2 m/s at 108 m, and then decreases to 10.5 m/s at 200 m. The corresponding velocity at 10 s is shown in Fig. 8 and given in Table 6. With $\varsigma = 0.1$, at 1 m the velocity is 11.7 m/s, increases to 13.6 m/s at 138 m, and then decreases to 11.7 m/s at 200 m. With $\varsigma = 0.5$, the velocity is 12.0 m/s at 1 m, increases to 14.1 m/s at 154 m, and then decreases to 12.1 m/s at 200 m.

6.3. PW model velocity behavior using the Greenshields distribution

The velocity with the PW model at 1 s over the 200 m circular road with $C_0 = 5$ m/s, $C_0 = 15$ m/s and $C_0 = 20$ m/s, and the Greenshields equilibrium velocity distribution is given in Fig. 9 and Table 7. With $C_0 = 5$ m/s, the velocity is 13.8 m/s at 1 m and approximately 21.7 m/s from 50 m to 72 m. It then decreases to approximately 11.1 m/s from 146 m to 174 m and is 13.4 m/s at 200 m. With $C_0 = 15$ m/s, at 1 m the velocity is 14.9 m/s and is 24.5 m/s at 44 m. It then decreases to approximately 11.9 m/s from 144 m to 164 m and is 14.5 m/s at 200 m. With $C_0 = 20$ m/s, at 1 m the velocity is 15.9 m/s and increases to 27.0 m/s at 46 m. It then decreases to approximately 11.0 m/s from 140 m to 160 m and is 15.4 m/s at 200 m. The corresponding velocity at 5 s is shown in Fig. 10 and given in Table 7. With $C_0 = 5$ m/s, at 1 m the velocity is 12.8 m/s and increases to 20.3 m/s at 124 m. It decreases to 12.4 m/s at 188 m and then increases to 12.7 m/s at 200 m. With $C_0 = 15$ m/s, at 1 m the velocity is 13.4 m/s and increases to 20.1 m/s at 110 m. It then decreases to 13.4 m/s at 200 m. With $C_0 = 20$ m/s, at 1 m the velocity is 13.8 m/s, increases to 19.8 m/s at 100 m, and then decreases to 13.7 m/s at 200 m. The corresponding velocity at 10 s is shown in Fig. 11 and given in Table 7. With $C_0 = 5$ m/s, at 1 m the velocity is 17 m/s and increases to 14.4 m/s at 44 m. It is 18.5 m/s at 174 m and then decreases to 17.3 m/s at 200 m. With $C_0 = 15$ m/s, at 1 m the velocity is 16.7 m/s and decreases to 14.9 m/s at 46 m. It is 18.1 m/s and 16.5 m/s at 162 m and 200 m, respectively. With $C_0 = 20$ m/s, the velocity is 16.1 m/s at 1 m and decreases to 15.2 m/s at 42 m. It is 17.8 m/s and 16.2 m/s at 150 m and 200 m, respectively.

The velocity behavior with the PW model for 10 s over a 200 m circular road with $C_0 = 15$ m/s, $C_0 = 20$ m/s and $C_0 = 50$ m/s is given in Figs. 12–14, respectively. With $C_0 = 5$ m/s, the velocity is between the

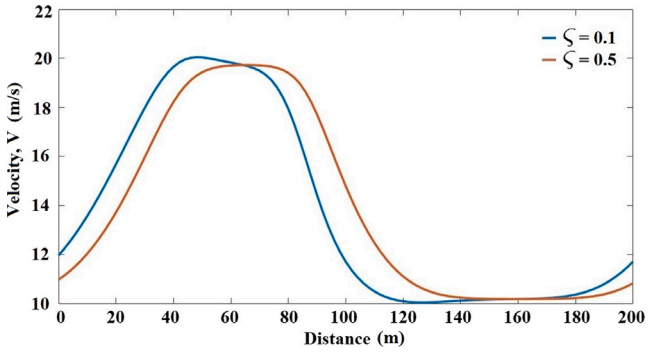

Fig. 6. The proposed model velocity over a 200 m circular road at 1 s with $\varsigma = 0.1$ and $\varsigma = 0.5$, and target equilibrium velocity distribution given by (4).

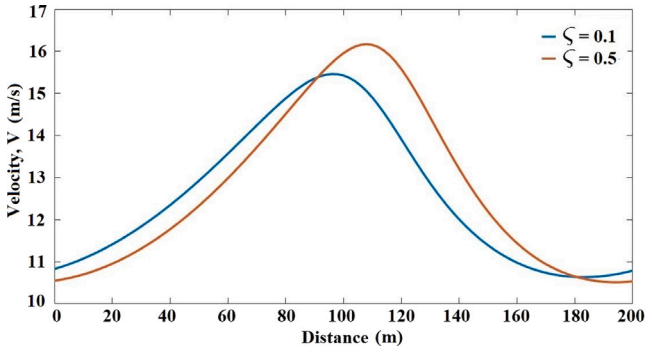

Fig. 7. The proposed model velocity over a 200 m circular road at 5 s with $\varsigma = 0.1$ and $\varsigma = 0.5$, and target equilibrium velocity distribution given by (4).

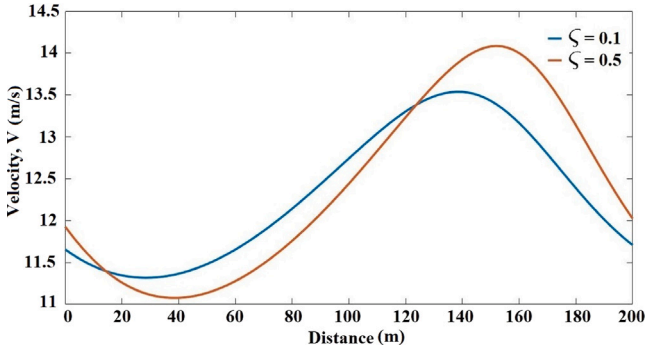

Fig. 8. The proposed model velocity over a 200 m circular road at 10 s with $\varsigma = 0.1$ and $\varsigma = 0.5$, and target equilibrium velocity distribution given by (4).

Table 6
The proposed model velocity with $\varsigma = 0.1$ and $\varsigma = 0.5$ at 1 s, 5 s, and 10 s, and target equilibrium velocity distribution given by (4).

Time (s)	ς	Distance (m)	Velocity (m/s)
1	0.1	1	12.0
1	0.1	48	20.1
1	0.1	126	10.1
1	0.1	200	11.7
1	0.5	1	11.0
1	0.5	70	19.8
1	0.5	146–178	10.3
1	0.5	200	10.9
5	0.1	1	10.8
5	0.1	98	15.5
5	0.1	200	11.0
5	0.5	1	10.6
5	0.5	108	16.2
5	0.5	200	10.5
10	0.1	1	11.7
10	0.1	138	13.6
10	0.1	200	11.7
10	0.5	1	12.0
10	0.5	154	14.1
10	0.5	200	12.1

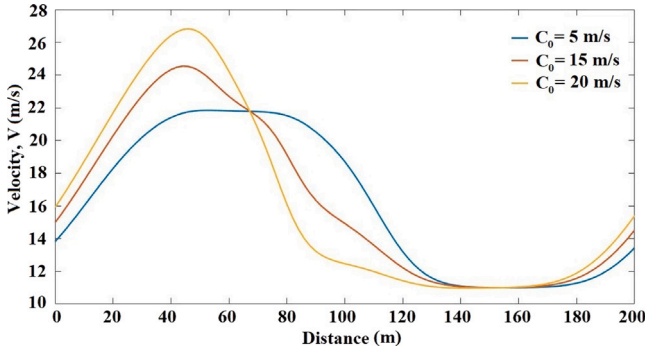

Fig. 9. The PW model velocity over a 200 m circular road at 1 s with $C_0 = 5$ m/s, $C_0 = 15$ m/s, and $C_0 = 20$ m/s, and the Greenshields equilibrium velocity distribution.

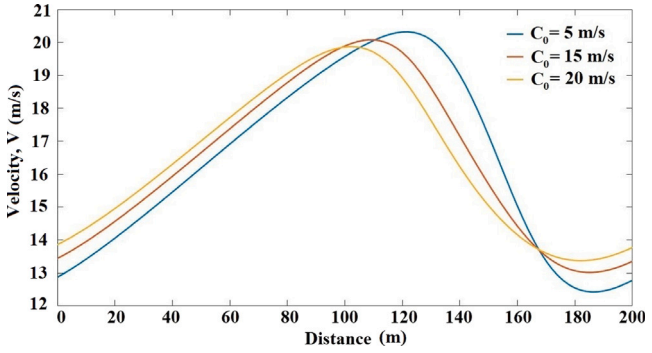

Fig. 10. The PW model velocity over a 200 m circular road at 5 s with $C_0 = 5$ m/s, $C_0 = 15$ m/s, and $C_0 = 20$ m/s, and the Greenshields equilibrium velocity distribution.

maximum and minimum as shown in Figs. 9–11. However, this value of C_0 is small as the velocity of non-homogeneous traffic is often higher than 5 m/s. The velocity is as high as 24.5 m/s with $C_0 = 15$ m/s at 1 s as shown in Fig. 9. Moreover, the results in Fig. 12 are unrealistic as there are very rapid changes in velocity which is impossible. With $C_0 = 20$ m/s, the velocity behavior is worse as shown in Fig. 13. At 1 s, the velocity reaches 27.0 m/s which is greater than the maximum value

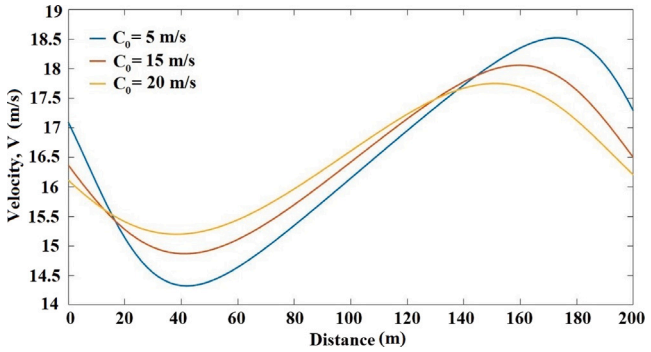

Fig. 11. The PW model velocity over a 200 m circular road at 10 s with $C_0 = 5$ m/s, $C_0 = 15$ m/s, and $C_0 = 20$ m/s, and the Greenshields equilibrium velocity distribution.

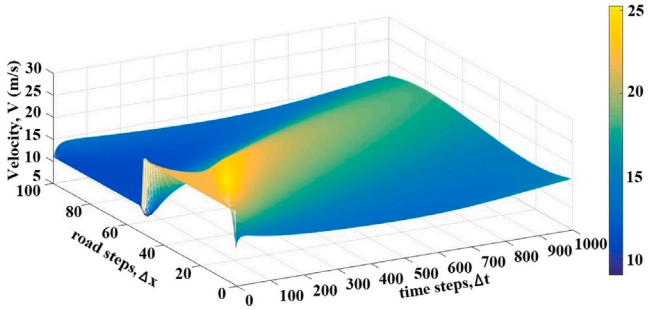

Fig. 12. Velocity evolution with the PW model for 10 s over a 200 m circular road with $C_0 = 15$ m/s, and the Greenshields equilibrium velocity distribution.

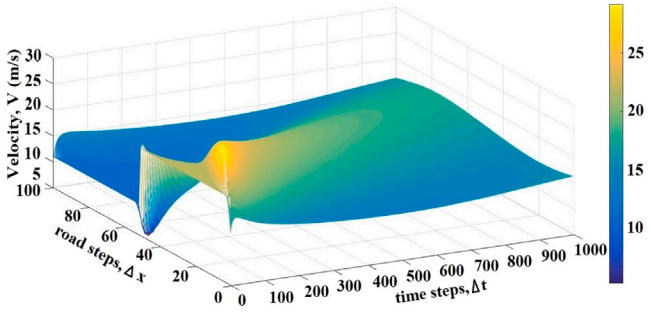

Fig. 13. Velocity evolution with the PW model for 10 s over a 200 m circular road with $C_0 = 20$ m/s, and the Greenshields equilibrium velocity distribution.

23.0 m/s. This indicates that the PW model can produce very unrealistic results. Further, with $C_0 = 50$ m/s, velocities over 75 m/s and below −37 m/s occur as shown in Fig. 14. This confirms earlier results that the velocity can exceed the limits with the PW model.

The proposed model was evaluated using two velocity distributions obtained from actual traffic data. The results for the equilibrium velocity distribution given by (8) at 1 s, 5 s and 10 s are presented in Figs. 3–5, respectively. This shows that the velocity variations are smooth and the velocity is within the minimum and maximum values. The results for the equilibrium velocity distribution given by (4) at 1 s, 5 s and 10 s are presented in Figs. 6–8, respectively. This also shows that the velocity variations are smooth and the velocity is within the minimum and maximum values. Thus, the proposed model produces much better results than the PW model.

The methodology employed in this paper can be used to realistically characterize non-homogeneous traffic. The proposed model is based on parameters derived from traffic physics and can be used to evaluate traffic behavior under different conditions by changing these parameters. This will be useful in applications such as traffic planning

Table 7
The PW model velocity with $C_0 = 5$ m/s, $C_0 = 15$ m/s and $C_0 = 20$ m/s at 1 s, 5 s, and 10 s, and the Greenshields equilibrium velocity distribution.

Time (s)	C_0 (m/s)	Distance (m)	Velocity (m/s)
1	5	1	13.8
1	5	50–72	21.7
1	5	146–174	11.1
1	5	200	13.4
1	15	1	14.9
1	15	44	24.5
1	15	144–146	11.0
1	15	200	14.5
1	20	1	15.9
1	20	46	27.0
1	20	140–160	11.0
1	20	200	15.4
5	5	1	12.8
5	5	124	20.3
5	5	188	12.4
5	5	200	12.7
5	15	1	13.4
5	15	110	20.1
5	15	200	13.4
5	20	1	13.8
5	20	100	19.8
5	20	200	13.7
10	5	1	17.1
10	5	44	14.4
10	5	174	18.5
10	5	200	17.3
10	15	1	16.7
10	15	46	14.9
10	15	162	18.1
10	15	200	16.5
10	20	1	16.1
10	20	42	15.2
10	20	150	17.8
10	20	200	16.2

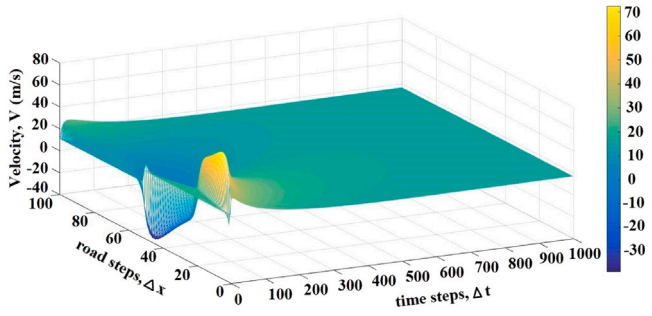

Fig. 14. Velocity evolution with the PW model for 10 s over a 200 m circular road with $C_0 = 50$ m/s, and the Greenshields equilibrium velocity distribution.

to improve road efficiency and reduce exhaust emissions. It can also be employed to evaluate the effects of imposing lane discipline when traffic is non-homogeneous.

7. Conclusion

In this paper, a macroscopic traffic flow model was proposed which considers harmonization during transitions. Parameters such as velocity, reaction time, harmonization time, and lateral distance headway were incorporated into this model. Thus, the proposed model can be used to evaluate traffic flow for different stimuli which is not possible with the PW model. Equilibrium velocity distributions were developed for non-homogeneous traffic based on recorded data. The results presented indicate that the PW model results in unrealistic traffic behavior with velocities beyond the limits. Conversely, the results with the proposed model are smooth and within the limits. Thus, this model can be used to characterize non-homogeneous traffic to provide realistic insights into traffic dynamics under different conditions.

CRediT authorship contribution statement

Waheed Imran: Conceptualization, Methodology, Software, Data curation, Writing – original draft, Visualization, Investigation, Validation, Writing – review & editing. **Zawar H. Khan:** Conceptualization, Methodology, Data curation, Writing – original draft, Supervision, Software, Validation, Writing – review & editing. **T. Aaron Gulliver:** Conceptualization, Methodology, Software, Supervision, Writing – review & editing. **Muhammad Alam:** Software, Validation. **Khurram S. Khattak:** Software, Validation.

Declaration of competing interest

The authors declare that they have no known competing financial interests or personal relationships that could have appeared to influence the work reported in this paper.

Data availability

Data will be made available on request.

References

Aw, A., Rascle, M., 2000. Resurrection of "second order" models of traffic flow. SIAM J. Appl. Math. 60 (3), 916–938.
Basak, K., et al., 2013. Modeling reaction time within a traffic simulation model. In: Proceedings of the IEEE International Conference on Intelligent Transportation Systems. The Hague, Nethrlands.
Bonzani, I., Mussone, L., 2009. On the derivation of the velocity and fundamental traffic flow diagram from the modelling of the vehicle–driver behaviors. Math. Comput. Modelling 50 (7–8), 1107–1112.
Brackstone, M., McDonald, M., 2007. Driver headway: How close is too close on a motorway? Ergonomics 50 (8), 1183–1195.
Cantarella, G.E., Luca, S.D., Gangi, M.D., Di Pace, R., Memoli, S., 2014. Macroscopic vs. mesoscopic traffic flow models in signal setting design. In: Proceedings of the International IEEE Conference on Intelligent Transportation Systems. Qingdao, China.
Daganzo, C.F., 1995. Requiem for second-order fluid approximations of traffic flow. Transp. Res. B 29 (4), 277–286.
Del Castillo, J.M., Pintado, P., Benitez, F.G., 1994. The reaction time of drivers and the stability of traffic flow. Transp. Res. B 28 (1), 35–60.
Delitala, M., Tosin, A., 2007. Mathematical modeling of vehicular traffic: A discrete kinetic theory approach. Math. Models Methods Appl. Sci. 17 (06), 901–932.
Devore, J.L., 2011. Simple linear regression and correlation. In: Probability and Statistics for Engineering and the Sciences, 8th ed. Brooks/Cole, Boston, MA, pp. 468–522 (Chapter 12c).
Grace, M.J., Potts, R.G., 1964. A theory of the diffusion of traffic platoons. Oper. Res. 12 (2), 255–275.
Graham, E.F., Chenu, D.C., 1962. A study of unrestricted platoon movement of traffic. Traffic Eng. 32 (7), 11–13.
Greenberg, H., 1959. An analysis of traffic flow. Oper. Res. 7 (1), 79–85.
Hegyi, A., De Schutter, B., Hellendoorn, J., Hoogendoorn, S.P., Tampère, C., 2001. Gelijke behandeling voor verkeersstroom modellen Kiezen voor golven, stromen of beweging. Verkeerskunde 52 (4), 32–36.
Helbing, D., 1996. Derivation and empirical validation of a refined traffic flow model. Physica A 233 (1–2), 253–282.
Henein, C.M., White, T., 2010. Microscopic information processing and communication in crowd dynamics. Physica A 389 (21), 4636–4653.
Hoogendoorn, S., Bovy, P.H.L., 2001. State-of-the-art of vehicular traffic flow modelling. Proc. Inst. Mech. Eng. I 215 (4), 283–303.
Imran, W., Khan, Z.H., Gulliver, T.A., Khattak, K.S., Nasir, H., 2020. A macroscopic traffic model for heterogeneous flow. Chinese J. Phys. 63, 419–435.
Jiang, R., Wu, Q., Zhu, Z., 2002. A new continuum model for traffic flow and numerical tests. Transp. Res. B 36 (5), 405–419.
Kerner, B.S., Konhäuser, P., 1993. Cluster effect in initially homogeneous traffic flow. Phys. Rev. E 48 (4), R2335.

Kessels, F., 2019. Traffic Flow Modeling. Springer, Cham, Switzerland, pp. 99–105.
Khan, Z.H., Gulliver, T.A., 2018. A macroscopic traffic model for traffic flow harmonization. Eur. Transp. Res. Rev. 10 (2), 30.
Khan, Z.H., Gulliver, T.A., 2019. A macroscopic traffic model based on anticipation. Arab. J. Sci. Eng. 44 (5), 5151–5163.
Khan, Z.H., Gulliver, T.A., 2020. A macroscopic traffic model based on transition velocities. J. Comput. Sci. 43, 101131.
Khan, Z.H., Gulliver, T.A., Imran, W., Khattak, K.S., Altamimi, A.B., Qazi, A., 2022a. A macroscopic traffic model based on relaxation time. Alex. Eng. J. 61, 585–596.
Khan, Z.H., Gulliver, T.A., Khattak, K.S., Qazi, A., 2019a. A macroscopic traffic model based on reaction velocity. Iran. J. Sci. Technol. Trans. Civ. Eng. 44 (1), 139–150.
Khan, Z.H., Imran, W., Azeem, S., Khattak, K.S., Gulliver, T.A., Aslam, M.S., 2019b. A macroscopic traffic model based on driver reaction and traffic stimuli. Appl. Sci. 9 (14), 2848.
Khan, Z.H., Imran, W., Gulliver, T.A., Khattak, K.S., Wadud, Z., Khan, A.N., 2020. An anisotropic traffic model based on driver interaction. IEEE Access 8, 66799–66812.
Khan, D., Khan, Z.H., Imran, W., Khattak, K.S., Gulliver, T.A., 2022b. Macroscopic flow characterization at T-junctions. Transp. Res. Interdiscip. Perspect. 14, 100591.
Khan, M.U., Saeed, S., Nehdi, M.L., Rehan, R., 2021. Macroscopic traffic-flow modelling based on gap-filling behavior of heterogeneous traffic. Appl. Sci. 11 (9), 4278.
Khan, Z.H., Shah, S.A.A., Gulliver, T.A., 2018. A macroscopic traffic model based on weather conditions. Chin. Phys. B 27 (7), 070202.
Kuhne, R.D., Rodiger, M.B., 1991. Macroscopic simulation model for freeway traffic with jams and stop-start waves. In: Winter Simulation Conference Proceedings. Phoenix, AZ, USA.
Li, J., Zhang, H.M., 2011. Fundamental diagram of traffic flow. Transp. Res. Rec. J. Transp. Res. Board 2260 (1), 50–59.
Lighthill, M.J., Whitham, G.B., 1955. On kinematic waves II. A theory of traffic flow on long crowded roads. Proc. R. Soc. Lond. Ser. A Math. Phys. Eng. Sci. 229 (1178), 317–345.
Liu, G., Lyrintzis, A., Michalopoulos, P., 1998. Improved high-order model for freeway traffic flow. Transp. Res. Rec. J. Transp. Res. Board 1644 (1), 37–46.
Maerivoet, S., De Moor, B., 2008. Transportation Planning and Traffic Flow Models. Katholieke Universiteit Leuven, Belgium.
Mallikarjuna, C., Rao, K., 2011. Heterogeneous traffic flow modeling: A complete methodology. Transportmetrica 7 (5), 321–345.
Mi, J., Bai, Y., Luo, M., Wang, H., Chen, M., 2019. Microscopic estimation of road impedance by decomposing traffic delay into individual road segments: An analytical approach. Math. Probl. Eng. 2019, 3285498.
Morgan, J.V., 2002. Numerical Methods for Macroscopic Traffic Models (Ph.D. dissertation). Dept. Math. Univ. Reading, Berkshire, UK.
de Moura, C.A., Kubrusly, C.S., 2013. The Courant–Friedrichs–Lewy (CFL) Condition: 80 Years After Its Discovery. Springer, Berlin.
Nagel, K., Wagner, P., Woesler, R., 2003. Still flowing: Approaches to traffic flow and traffic jam modeling. Oper. Res. 51 (5), 681–710.
National Highways of Pakistan, Downloads.nha.gov.pk, [Online]. Available: http://downloads.nha.gov.pk. (Accessed 6 August 2018).
Papageorgiou, M., 1998. Some remarks on macroscopic traffic flow modeling. Transp. Res. A 32 (5), 323–329.
Papageorgiou, M., Blosseville, J.-M., Hadj-Salem, H., 1989. Macroscopic modelling of traffic flow on the Boulevard Peripherique in Paris. Transp. Res. B 23 (1), 29–47.
Payne, H.J., 1971. Models of freeway traffic and control. Math. Models Public Syst. (Simul. Counc. Proc.) 1, 51–61.
Phillips, W.F., 1979. A kinetic model for traffic flow with continuum implications. Transp. Plan. Technol. 5 (3), 131–138.
Qu, D., Chen, X., Yang, W., Bian, X., 2014. Modeling of car-following required safe distance based on molecular dynamics. Math. Probl. Eng. 604023 (2014).
Richards, P.I., 1956. Shock waves on the highway. Oper. Res. 4 (1), 42–51.
Richardson, A.D., 2012. Refined Macroscopic Traffic Modelling Via Systems of Conservation Laws (Master's thesis). Dept. Math. and Stats., Univ. Victoria, Vicotria, BC, Canada.
Salter, R.J., 1996. The relationship between speed, flow and density of a highway traffic stream. Highw. Traffic Anal. Des. 119–130.
Timilsina, G.R., Dulal, H.B., 2010. Urban road transportation externalities: Costs and choice of policy instruments. World Bank Res. Obs. 26 (1), 162–191.
Toro, E.F., 2011. Riemann Solvers and Numerical Methods for Fluid Dynamics: A Practical Introduction. Springer, Berlin.
Whitham, G.B., 1971. Linear and Nonlinear Waves. Wiley, New York, NY, USA.
Xin, Z., Xu, J., 2015. Synchronization transition and traffic congestion in one-dimensional traffic model. Abstr. Appl. Anal. 2015, 167430.
Yi, P., Lu, J., Zhang, Y., Lu, H., 2004. Safety-based capacity analysis for Chinese highways. IATSS Res. 28 (1), 47–55.
Yu, C., Zhang, J., Yao, D., Zhang, R., Jin, H., 2016. Speed-density model of interrupted traffic flow based on coil data. Mob. Inf. Syst. 2016, 7968108.
Zhang, H., 1998. A theory of non-equilibrium traffic flow. Transp. Res. B 32 (7), 485–498.